Magnetic interface states in graphene-based quantum wires

J. Milton Pereira, Jr.,[1,2] F. M. Peeters,[1] and P. Vasilopoulos[3]

[1]*Department of Physics, University of Antwerp, Groenenborgerlaan 171, B-2020 Antwerpen, Belgium*
[2]*Departamento de Física, Universidade Federal do Ceará, Fortaleza, Ceará 60455-760, Brazil*
[3]*Department of Physics, Concordia University, Montreal, Quebec, Canada H3G 1M8*

The electron states of a finite-width graphene sheet in the presence of an electrostatic confining potential and a perpendicular magnetic field are investigated. The confining potential shifts the Landau levels inside the well and creates current-carrying states at or close to the interface with the potential barriers in addition to the edge states caused by the finite width of the sheet. Detailed energy spectra are given as a function of the quantum wire parameters. The dependence of the density of states on the confinement potential is evaluated for finite and zero magnetic fields.

PACS number(s): 73.21.−b, 71.10.Pm, 81.05.Uw

I. INTRODUCTION

The recent production of single layers of stable carbon crystals[1–3] has attracted much interest in their fundamental properties and their potential technological applications. The unusual properties of carriers in graphene are a consequence of the gapless and approximately linear electron dispersion at the vicinity of the Fermi level at two inequivalent points of the Brillouin zone. In the low-energy limit, the quasiparticles in these systems are described in terms of massless chiral relativistic fermions governed by the Dirac equation. In particular, graphene has been shown to display an unusual quantum Hall effect,[4–8] in which the quantum Hall plateaus are found in half-integer multiples of 4. This results from the fourfold degeneracy of the Landau levels (LLs) along with the existence of a nonzero Berry phase. The edge states in graphene in a perpendicular magnetic field have been previously investigated theoretically for thin graphene strips,[9,10] where they were also found to display unusual properties, such as counterpropagating spin-polarized modes.

Another important result concerning single graphene layers is the possibility of controlling the electron density and Fermi level by a gate voltage. This allows the creation of graphene-based quantum structures such as potential barriers and quantum wires (QWs). Theoretical studies have shown that the relativistic behavior of quasiparticles in graphene allows the observation of effects such as the Klein paradox, which is the perfect transmission of relativistic particles across potential barriers, as well as a direction-dependent tunneling through barriers.[11–15] In addition, recent experimental work has demonstrated electronic confinement in patterned graphene structures created by standard lithography methods.[16]

The fact that the interaction of charge carriers with electrostatic potential barriers in graphene is quite distinct from that in nonrelativistic systems allows one to expect that the presence of barrier interfaces may create propagating states which differ significantly from the usual edge states. In this paper, we investigate such states by considering the interplay of an electrostatic potential barrier and an external magnetic field perpendicular to a graphene QW. We thus demonstrate the existence of propagating interface states and show that

they display properties that contrast markedly with the ordinary edge states.

This paper is organized as follows. In Sec. II, we present the model and formalism and in Sec. III numerical results. We conclude with remarks in Sec. IV.

II. MODEL AND FORMALISM

The crystal structure of undoped, defect-free graphene layers is that of a honeycomb lattice of covalent-bond carbon atoms. To each carbon atom corresponds a valence electron, and the structure can be described as composed of two sublattices, labeled A and B. The low-energy excitations of the system at the vicinity of the **K** point and in the presence of both an electrostatic potential U and a uniform magnetic field B perpendicular to the plane of the graphene sheet are described, in the continuum approximation, by the two-dimensional (2D) Dirac equation

$$\{v_F[\vec{\sigma} \cdot \hat{\mathbf{p}} - e\mathbf{A}] + mv_F^2\sigma_z\}\Psi = (E - U)\Psi, \qquad (1)$$

where the pseudospin matrix $\vec{\sigma}$ has components given by Pauli's matrices, and $\hat{\mathbf{p}} = (p_x, p_y)$ is the momentum operator. The "speed of light" of the system is v_F, the Fermi velocity ($v_F \approx 1 \times 10^6$ m/s), and **A** is the vector potential. The eigenstates of Eq. (1) are represented by two-component spinors $\Psi = [\psi_A, \psi_B]^T$, where ψ_A and ψ_B are the envelope functions associated with the probability amplitudes at the respective sublattice sites of the graphene sheet. The term $\propto mv_F^2$ introduces an energy gap, which may represent, e.g., the effect of spin-orbit coupling.

We now consider a narrow graphene layer, of width W, in the presence of a one-dimensional (1D) potential $U = U(x)$ and a perpendicular magnetic field B. This allows us to write the solutions for the spinor components in the form $\psi_A(x, y) = \phi_A(x)e^{ik_y y}$ and $\psi_B(x, y) = i\phi_B(x)e^{ik_y y}$ because of translational invariance along the y direction and the particular choice of Landau's gauge $\mathbf{A} = (0, Bx, 0)$. The resulting equations for $\phi_A(x)$ and $\phi_B(x)$ are

$$\frac{d\phi_A}{dx} - (k_y - eBx)\phi_A = -[E - U(x) + mv_f^2]\phi_B,$$

$$\frac{d\phi_B}{dx} + (k_y - eBx)\phi_B = [E - U(x) - mv_f^2]\phi_A. \quad (2)$$

These equations can be decoupled and, by setting $\xi = \beta^{1/2}(x - k_y/\beta)$, where $\beta = \ell_B^{-2} = eB/\hbar$ is the inverse magnetic length squared, the result is

$$d^2\phi_A/d\xi^2 + [(\Omega+1) - \xi^2]\phi_A - \frac{u'}{(\epsilon-u+\Delta)}(d\phi_A/d\xi + \xi\phi_A)$$

$$= 0, \quad (3)$$

$$d^2\phi_B/d\xi^2 + [(\Omega-1) - \xi^2]\phi_B + \frac{u'}{(\epsilon-u-\Delta)}(d\phi_B/d\xi - \xi\phi_B)$$

$$= 0, \quad (4)$$

where $\Omega = [(\epsilon-u)^2 - \Delta^2]/\beta$, $u = (\hbar v_F)^{-1}U$, $\epsilon = (\hbar v_F)^{-1}E$, $\Delta = mv_F/\hbar$, and the prime denotes derivative with respect to ξ. For a constant potential $U = U_0$, Eqs. (2) and (3) have well-known solutions in terms of Hermite polynomials and the spectrum is

$$E = \pm \hbar v_F \sqrt{2n\beta + \Delta^2} + U_0, \quad (5)$$

where n is an integer. This contrasts significantly with the nonrelativistic spectrum $E = \hbar\omega_c(n+1/2) + U_0$.

III. RESULTS

A. Dispersion relation and density of states

First, we consider the effect of a steep potential well $U(x)$, with a characteristic width L in a graphene strip of width $W \gg L$. In this case, the derivatives of the potential are strongly localized functions that have nonzero values only at the vicinity of the barrier interfaces. The solutions then depend on the width L and the strength of the magnetic field B through the ratio ℓ_B/L. Let us consider initially the case $2\ell_B/L \ll 0.5$, which corresponds to classical orbits that fit inside the QW. We can assume solutions of the form $\phi_C = f_C(\xi)e^{-\xi^2/2}$, $C = A, B$. For a constant potential, f_C are the well-known Hermite polynomials. Thus, for sufficiently strong B and small k_y, the spinor functions quickly decay with ξ and the solutions are, to a good approximation, localized inside the well. Therefore, the energy spectrum is dispersionless, and for small n it is the same as that of the LL for $U = 0$. For larger values of k_y, the center of the solutions $\ell_B^2 k_y$ is shifted toward the barrier regions. For the lowest LL ($n = 0$), one can estimate the limits of the central dispersionless region by setting $\exp(-\xi^2/2) \approx 0.1$, or $\xi \approx 2$, since in this case the amplitude of the wave function inside the barriers is negligible. This gives $-1 + 4\ell_B/L < 2k_y\ell_B^2/L < 1 - 4\ell_B/L$. For nonzero values of n, the central dispersionless region of the spectrum is expected to be narrower, since the spinor functions are less localized and can have a larger magnitude within the barrier regions.

For sufficiently large values of the momentum along the y direction, a similar argument shows that the energy levels may be accurately approximated by the LL shifted by U_0 in the regions $2k_y\ell_B^2/L < -1 - 4\ell_B/L$ and $2k_y\ell_B^2/L > 1 + 4\ell_B/L$.
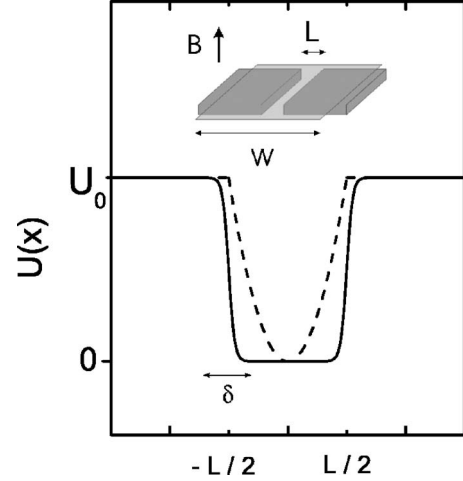

FIG. 1. Schematic depiction of the different potential well profiles discussed in the text: tangent hyperbolic (solid line) and parabolic (dashed line).

For intermediate values of k_y, one expects dispersive solutions. These solutions can be described as interface states in the sense that they are localized electron states in the x direction that propagate along the interfaces with the potential barriers, in analogy with the edge states of a 2D electron gas in a magnetic field, but with the fundamental difference that in the present case the spinor functions are non-negligible both inside the QW and in the barriers. These are current-carrying states and, for sufficiently smooth potentials, should not depend on the microscopic structure of the graphene sheet. For even larger values of k_y, the spinor functions may be shifted toward the edges of the sample and give rise to edge states, which have been shown to depend on the shape of the graphene edges.[17]

We have considered two specific types of potential wells, as shown in Fig. 1. The solid line illustrates the step potential given by

$$U(x) = \frac{U_0}{2}\{\tanh[(-x-L/2)/\delta] + \tanh[(x-L/2)/\delta] + 2\},$$

$$(6)$$

where δ denotes the thickness of the interface. The dashed line in Fig. 1 refers to a parabolic potential

$$U(x) = \begin{cases} U_0(2x/L)^2, & |x| < L/2 \\ U_0, & |x| > L/2. \end{cases} \quad (7)$$

Figure 2 shows numerical results for the energy spectrum of a QW with the potential given by Eq. (6). The results are for $L = 200$ nm and an interface width of 10 nm, which is much larger than the lattice parameter of graphene $a \approx 0.14$ nm, $B = 2$ T, and $U_0 = 50$ meV. In this case, we have $2\ell_B/L \approx 0.18$. The vertical dashed lines delimit the range $1 - 4\ell_B/L < |2k_y\ell_B^2/L| < 1 + 4\ell_B/L$. In contrast with conventional edge states, the barrier interface does not cause a splitting of the dispersion branches. This is a consequence of the difference in boundary conditions at the potential interfaces and the edges of the graphene sheet; i.e., at the potential step,
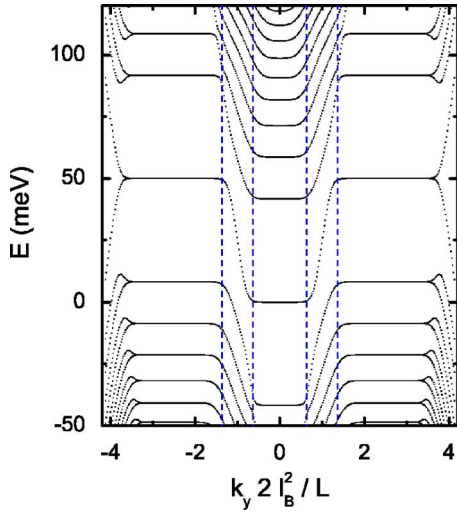
FIG. 2. (Color online) Energy spectrum of a graphene QW with armchair edges for $B=2$ T and in the presence of a potential given by Eq. (6), with $U_0=50$ meV and $L=200$ nm.

the wave function is finite and continuous and the associated probability density can be significant for $|x| > L/2$, whereas at the edges of the sample, as in the case of a graphene sheet with an armchair termination, the wave function was assumed to vanish. Alternatively, one could use boundary conditions appropriate to a graphene sheet with zigzag edges. This is equivalent to setting the spinor function to zero at a single sublattice. A detailed comparison between edge states in each case has been done in Ref. 17.

For comparison, Fig. 3 shows the spectrum of a parabolic confining potential given by Eq. (7). This potential is nonzero at every point, except at $x=0$, which is the reason why the states are dispersive for all values of k_y satisfying $|2k_y\ell_B^2/L| < 1$. This result becomes similar to that of the tangent hyperbolic potential for large δ.

For weaker fields, such that $2\ell_B/L > 0.5$, the former picture breaks down and the magnetic field acts as a perturbation to the zero-field case.[12] For $B=0$, the electron states inside the QW that propagate perpendicularly to the barrier interfaces are transmitted without reflection (Klein
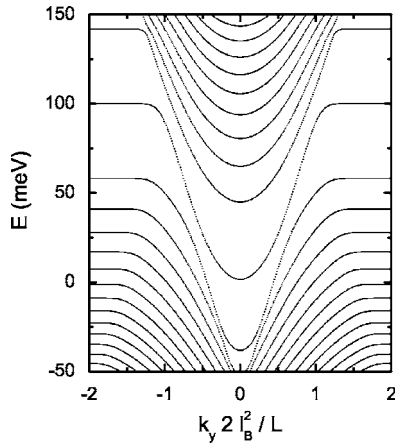

FIG. 3. The same as Fig. 2 but for a parabolic potential given by Eq. (7), with $U_0=100$ meV, $L=200$ nm, and $B=2$ T.
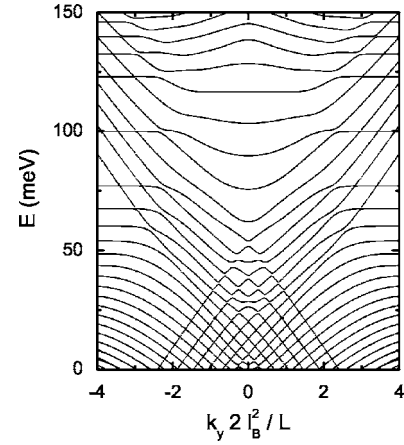
tunneling).[11–14] This counterintuitive behavior results from the absence of a gap in the spectrum and from the chiral nature of the quasiparticles in graphene. However, recently it has been demonstrated that nonzero values of momentum along y allow the existence of confined electron states in a QW.[12] For large values of k_y, the dispersion branches are given approximately by

$$E = \hbar v_F [(\ell\pi/L)^2 + k_y^2]^{1/2}, \qquad (8)$$

where ℓ is an integer. As a finite magnetic field is introduced, one can expect a modification of these states. In particular, one expects the existence of localized states at $k_y=0$. This situation is observed in Fig. 4, where the energy spectrum is plotted as a function of wave vector, for the potential given by Eq. (6), with $U_0=100$ meV, $L=100$ nm, $W=800$ nm, and $B=0.6$ T. This case corresponds to $2\ell_B/L \approx 0.66$. The figure shows the existence of dispersive states for a wide range of wave vectors, as well as dispersionless branches that correspond to the shifted LLs at the barriers.

For small energies and wave vectors, the results for $B=0$ show the existence of hole states in the barriers that either propagate (Klein paradox) or tunnel through the well. For a finite field, in a semiclassical description, the trajectories of the holes would be deflected by the magnetic field and would be confined into closed orbits that cross the QW. A similar behavior is thus obtained for energies close to zero, as shown in Fig. 5. The figure shows the wave functions [left, panels (a) and (c)] and the respective probability densities [right, panels (b) and (d)] for two states with $k_y=0$ in a QW with the same parameters as in Fig. 4 and two energies: $E=2.03$ meV (upper panels) and $E=0$ (lower panels). The higher-energy state describes holes that cross the well region via electron-hole conversion and thus show a maximum in the probability density inside the well, whereas the result for zero energy corresponds to holes that tunnel across the well region and are confined by the magnetic field. For higher-energy eigenstates and $k_y=0$, the wave functions show an oscillatory behavior inside the potential well and quickly decay in the barriers. Therefore, these states possess a dominant electronlike character.
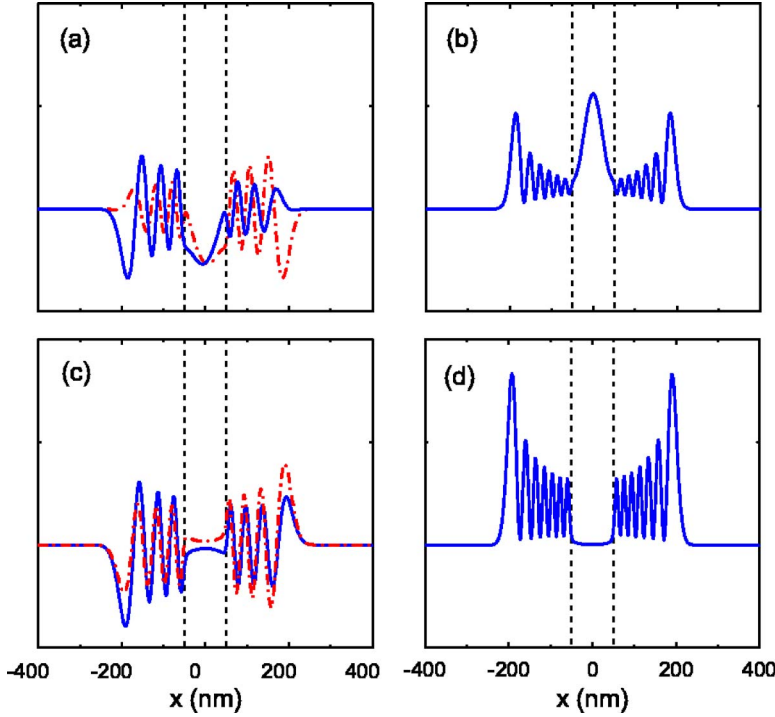

FIG. 4. The same as Fig. 2 but now with $U_0=100$ meV, $L=100$ nm, and a smaller magnetic field $B=0.6$ T.

FIG. 5. (Color online) Wave functions (left panels: ϕ_A, solid; ϕ_B, dashed-dotted) and the respective probability densities (right panels) for two low-energy states of Fig. 4. Upper panels, $E=2.03$ meV; lower panels, $E=0$ meV.

For finite values of k_y, the spectrum displays dispersive branches with either positive or negative slopes. The wave functions in these cases have non-negligible amplitudes inside the potential well and in the barriers, and thus are associated with propagating electrons and holes. On the other hand, the states associated with flat energy branches have finite amplitudes inside the barriers. The propagating states are found to interact with the dispersionless states, with the appearance of anticrossings.

The right part of Fig. 6 shows plots of ϕ_A for electron states at the proximity of a specific anticrossing for the situation corresponding to Fig. 4 that is shown enlarged in the left part of the figure. The results for points (a) and (b) ($k_y 2\ell_B^2/L=2.19$) indicate that close to the anticrossings, the electron states are a superposition of oscillatory states (inside
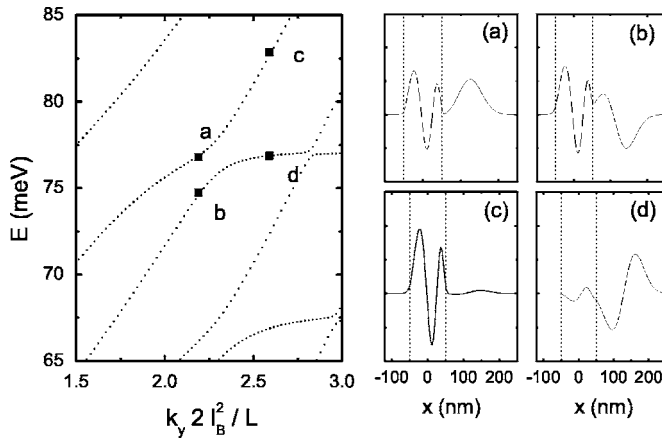

FIG. 6. Left: A zoom of the electron dispersion branches of Fig. 4 at the vicinity of an anticrossing; the parameters are given in the text. Right, (a)–(d): Spinor component ϕ_A for some particular states specified in the text.

the QW) and nonpropagating states (at the barriers), whereas away from the anticrossings ($k_y 2\ell_B^2/L=2.59$), the wave functions match the results for either confined states (c) in the QW or LLs (d) in the barriers. The vertical lines (dotted) in these figures delimit the QW region.

In the calculation of several physical quantities, the density of states (DOS) is needed, which is defined as

$$\rho(E) = \frac{1}{S}\sum_{k_x,k_y}\sum_n \delta(E - E_n(k_y)), \tag{9}$$

where $S=WL$ is the total area of the sample and n labels the different energy branches. The summation over k_x is replaced by an integral, and we obtain

$$\rho(E) = \frac{WE_0}{(2\pi\ell_B)^2}\sum_n \int_{-\infty}^{\infty} \frac{\Gamma/\pi}{[E - E_n(k_y)]^2 + \Gamma^2}dk_y, \tag{10}$$

where we introduced broadening of the energy levels by replacing the δ functions with Lorentzians of constant width Γ; $E_0=\sqrt{2e\hbar B}$ denotes the characteristic energy scale of the system.

Figure 7 shows numerical results for the DOS for the hyperbolic tangent QW, with $U_0=50$ meV, $L=200$ nm and for different values of the external magnetic field: $B=0.5$ (dashed), 1.0 (dotted), 1.5 (dash-dotted), and 2.0 T (solid). In all cases, we used $\Gamma/E_0=28$. The figure shows that the presence of the barriers shifts the DOS peaks by U_0 from the zero potential results. In contrast with a conventional 2D electron gas, all DOS results for graphene show a pronounced peak at $E=50$ meV, whereas the remaining peaks are shifted according to the different values of B. This is a consequence of the fact that in graphene, the energy of the LL with index $n=0$ is independent of B. In addition, for each value of B extra peaks result from the LL inside the QW. Due to the square-
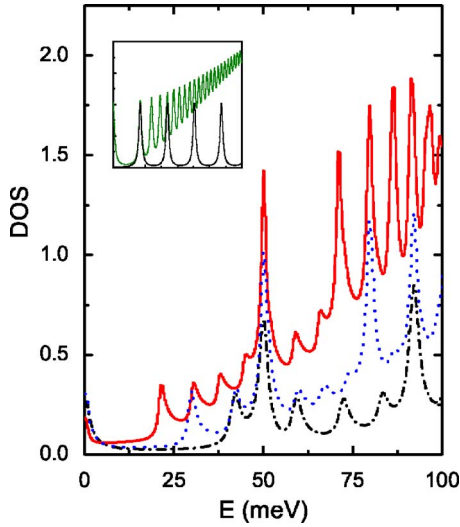
FIG. 7. (Color online) Density of states for a QW on graphene with U_0=50 meV and L=200 nm. B=0.5 T (dashed), B=1.0 T (dotted), B=1.5 T (dashed-dotted), and B=2.0 T (solid). Inset: Comparison between the DOS of a nonrelativistic electron gas (green) and the DOS of electrons in graphene (solid) for U_0=0.

root dependence of the spectrum [see Eq. (5)], the distance between the peaks decreases as the energy increases. Therefore, the influence of the LL in the QW becomes more evident for energies closer to zero. The inset contrasts the DOS of a nonrelativistic electron gas (green) with the DOS of electrons in graphene (solid), for U_0=0.

The dependence of the DOS on the barrier height U_0 is shown in Fig. 8, where L=200 nm and B=2 T, for different values of U_0, namely, U_0=0 (solid line), U_0=25 meV
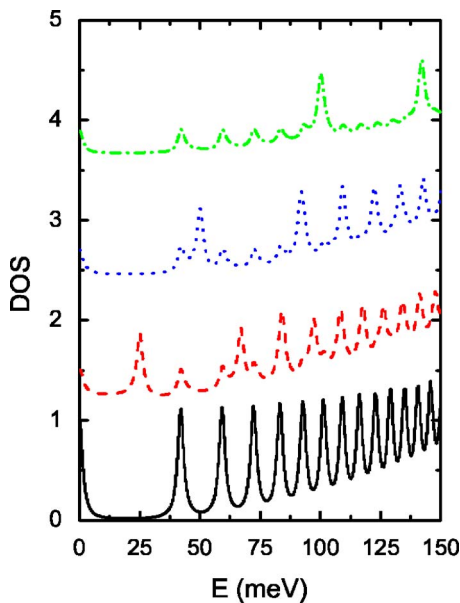

FIG. 8. (Color online) Density of states for a graphene QW with B=2 T and L=200 nm. The solid, dashed, dotted, and dashed-dotted curves correspond, respectively, to U_0=0, U_0=25 meV, U_0=50 meV, and U_0=100 meV. The last three curves are shifted up by 1.25 for clarity.
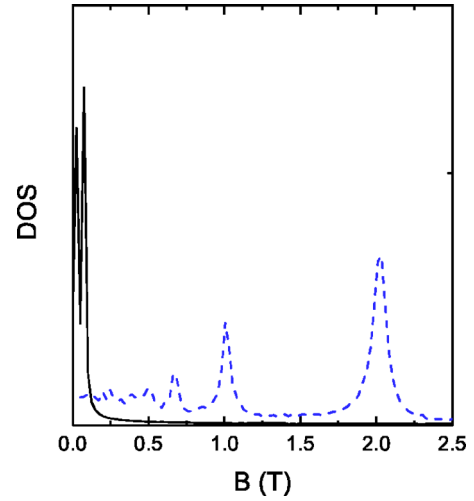

FIG. 9. (Color online) Density of states as a function of the magnetic field for E=8 meV, in the absence of a confining potential (black solid curve) and a graphene QW with U_0=50 meV (blue dashed curve). L=200 nm in both cases.

(dashed), U_0=50 meV (dotted), and U_0=100 meV (dotted-dashed). As the potential increases, there is a clear shift of the peaks from the values given by Eq. (5) with U_0=0, with the n=0 peak now shifted to the value of U_0. Also evident is the presence of states inside the QW, indicated by the existence of additional peaks, with positions that are independent of the potential step. These results indicate that due to the specific nature of the LL spectrum in graphene, one can increase the DOS at a particular energy by a suitable change of U_0 so that one LL outside the QW is matched with another LL inside the well. This condition (for Δ=0) is expressed as

$$U_0 = \hbar v_F (\sqrt{2n'\beta} - \sqrt{2n\beta}), \tag{11}$$

where n and n' are integers. This condition is shown in Fig. 8 in the result for U_0=25 meV, for the peak at E=84 meV, with n'=4 and n=2. Figure 9 shows the DOS as a function of the external magnetic field for E=8 meV, for U_0=0 (solid line) and U_0=50 meV (dashed line). The shift of the LL brought about by the potential barriers causes the appearance of several DOS peaks that are absent from the uniform system.

B. Energy spectrum versus QW parameters

Figure 10 shows the spectrum, as a function of the magnetic field, for two values of the wave vector, (a) k_y=0 and (b) k_y=0.1 nm^{-1}, for the QW potential of Eq. (6) with U_0=100 meV and L=100 nm. In both cases, the results show that the presence of the potential barriers introduces a significant modification of the energy eigenstates, in comparison with the results for U_0=0 (in which case the eigenvalues are proportional to the square root of the external magnetic field). Figure 10(b) shows the presence of the quantized confined states as B tends to 0. These discrete states are initially very weakly dependent on the external field. As the field increases, these states interact with the nonpropagating states, as evidenced by the presence of anticrossings. At
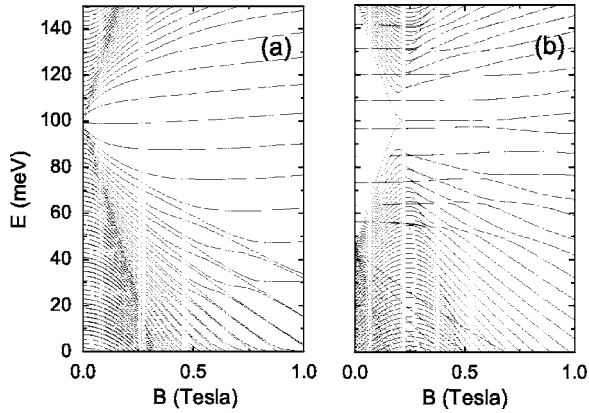
FIG. 10. Energy spectrum of a graphene QW with armchair edges as a function of the magnetic field B, with $U_0=100$ meV, $L=100$ nm, and (a) $k_y=0$ and (b) $k_y=0.1$ nm^{-1}.

small fields, the figure shows split branches, which are edge states that arise due to the fact that the spinor amplitudes are set to zero at the edges of the sample, whose width is $W=800$ nm. This corresponds to the boundary conditions of a graphene sheet with an armchair edge.

The left panel in Fig. 11 shows the dependence of the energy eigenvalues on the QW width, for $k_y=0$, $B=2$ T, and $U_0=100$ meV. The results show that the higher-energy levels are strongly modified even for wide wells, whereas the lower-lying states can be accurately described by Eq. (5) with $U_0=0$ for a relatively thin QW. The figure allows us to distinguish two regions in the spectrum, which arise due to the nonuniform distribution of the LLs in graphene. One region corresponds to the lower-energy states, which arise due to the strong interaction between the low-energy states in the well with the shifted negative-energy states in the barriers. The degeneracy of these states is lifted for small L and the spectrum shows an approximately linear dependence on the QW width. In particular, the interaction with the lower-energy states modifies the $E=0$ LL for $L \approx 80$ nm, which is equivalent to $2\ell_B/L \approx 0.45$. The other region corresponds to higher-energy states, which remain degenerate but are strongly shifted for small L. These states are weakly dependent on the well width for larger values of L, e.g., for $L > 120$ nm.

The dependence of the energy spectrum on the potential barrier height U_0 is shown in the right panel of Fig. 11 for $L=100$ nm, $B=2$ T, and $k_y=0$. As U_0 increases, the figure again shows the appearance of two sets of states: one comprises states that are weakly dependent on U_0 and the other, states that show a significant dependence on U_0. This is caused by the hole states in the barriers, whose energies are shifted by the potential. As U_0 increases, the LLs in the well region interact with the set of shifted LLs in the barriers, causing the appearance of additional electron states at energies close to zero.

IV. SUMMARY

In this work, we showed the effect of a confining 1D electrostatic potential on the energy spectrum of electrons in
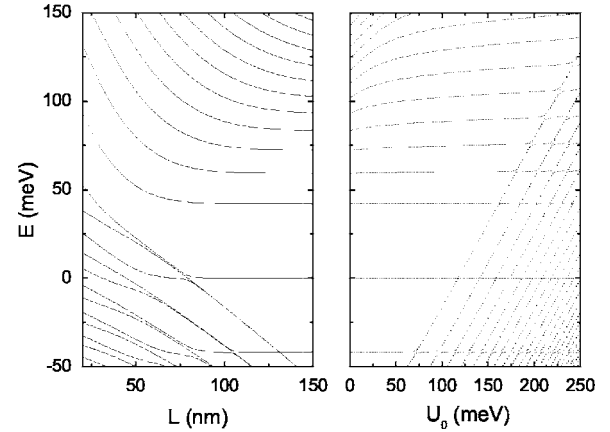

FIG. 11. Energy spectrum of a graphene QW for $B=2$ T and $k_y=0$. The spectrum is plotted vs the width L in the left panel, for $U_0=100$ meV, and vs the potential height U_0 in the right panel, for $L=100$ nm.

a graphene QW in the presence of a perpendicular magnetic field. We found a shift of the Landau levels caused by this potential, which may be observable by its effect on the quantum Hall steps in the presence of gate voltages. For steep potential barriers, there is a clear distinction between a low-magnetic-field regime, characterized by the existence of dispersive confined states with small wave vectors inside the QW as well as nonpropagating states in the barriers, and a higher-magnetic-field regime, in which there are nonpropagating states inside the well and outside the QW together with propagating states at the interfaces of the potential barriers. These interface states may cross the Fermi level and, together with the conventional edge states that arise due to the finite size of the sample, can contribute to the conductivity of the system. The modification of the LL spectrum in the QW is also evident in the shift of the peaks in the DOS in comparison with the results for zero confining potential, along with the appearance of additional peaks caused by the LLs inside the QW.

Experimental verification of these results may be accomplished by the fabrication of single layers of graphene on split-gate electrodes.[18–23] Previous studies have shown the feasibility of the production of mesoscopic devices of micron-size *graphite* disks (with 60–100 graphene layers) by means of focused-ion-beam lithography.[24] A similar approach may be suitable for the experimental investigation of magnetic interface states on a single layer of graphene.

[1] K. S. Novoselov, A. K. Geim, S. V. Morozov, D. Jiang, Y. Zhang, S. V. Dubonos, I. V. Grigorieva, and A. A. Firsov, Science **306**, 666 (2004).

[2] K. S. Novoselov, D. Jiang, F. Schedin, T. J. Booth, V. V. Khotkevich, S. V. Morozov, and A. K. Geim, Proc. Natl. Acad. Sci. U.S.A. **102**, 10451 (2005).

[3] Y. Zhang, J. P. Small, W. V. Pontius, and P. Kim, Appl. Phys. Lett. **86**, 073104 (2005).

[4] Y. Zheng and T. Ando, Phys. Rev. B **65**, 245420 (2002).

[5] V. P. Gusynin and S. G. Sharapov, Phys. Rev. Lett. **95**, 146801 (2005).

[6] K. S. Novoselov, A. K. Geim, S. V. Morozov, D. Jiang, M. I. Katsnelson, I. V. Grigorieva, S. V. Dubonos, and A. A. Firsov, Nature (London) **438**, 197 (2005).

[7] Y. Zhang, Y. W. Tan, H. L. Stormer, and P. Kim, Nature (London) **438**, 201 (2005).

[8] N. M. R. Peres, F. Guinea, and A. H. Castro Neto, Phys. Rev. B **73**, 125411 (2006).

[9] N. M. R. Peres, A. H. Castro Neto, and F. Guinea, Phys. Rev. B **73**, 241403(R) (2006).

[10] D. A. Abanin, P. A. Lee, and L. S. Levitov, Phys. Rev. Lett. **96**, 176803 (2006).

[11] O. Klein, Z. Phys. **53**, 157 (1929).

[12] J. M. Pereira, Jr., V. Mlinar, F. M. Peeters, and P. Vasilopoulos, Phys. Rev. B **74**, 045424 (2006).

[13] M. I. Katsnelson, K. S. Novoselov, and A. K. Geim, Nat. Phys. **2**, 620 (2006).

[14] V. V. Cheianov and V. I. Fal'ko, Phys. Rev. B **74**, 041403(R) (2006).

[15] J. Milton Pereira, Jr., F. M. Peeters, and P. Vasilopoulos (unpublished).

[16] C. Berger, Z. Song, X. Li, X. Wu, N. Brown, C. Naud, D. Mayou, T. Li, J. Hass, A. N. Marchenkov, E. H. Conrad, P. N. First, and W. A. de Heer, Science **312**, 1191 (2006).

[17] L. Brey and H. A. Fertig, Phys. Rev. B **73**, 195408 (2006).

[18] Y. Zhang, J. P. Small, M. E. S. Amori, and P. Kim, Phys. Rev. Lett. **94**, 176803 (2005).

[19] J. Reinhardt and W. Greiner, Rep. Prog. Phys. **40**, 219 (1977); V. Petrillo and Davide Janner, Phys. Rev. A **67**, 012110 (2003).

[20] P. R. Wallace, Phys. Rev. **71**, 622 (1947); M. Wilson, Phys. Today **59**(1), 21 (2006).

[21] G. W. Semenoff, Phys. Rev. Lett. **53**, 2449 (1984).

[22] I. A. Luk'yanchuk and Y. Kopelevich, Phys. Rev. Lett. **93**, 166402 (2004).

[23] C. L. Kane and E. J. Mele, Phys. Rev. Lett. **95**, 226801 (2005).

[24] E. Dujardin, T. Thio, H. Lezec, and T. Ebbesen, Appl. Phys. Lett. **79**, 2474 (2001).